Research Square

Preprints are preliminary reports that have not undergone peer review.
They should not be considered conclusive, used to inform clinical practice,
or referenced by the media as validated information.

High-sensitivity temperature sensing via color change: A study on the thermal coupling and non-thermal coupling energy levels in YVO 4 :Tm 3+ /Er 3+

Zhensheng Lu
Suihua University
Hongxia Tang
Suihua University
Meilin Song
Suihua University
Changxing Yu
Suihua University
Changwen Wang
wangchangwen1988@163.com

Suihua University

Research Article

Keywords: temperature sensing, thermal coupling, relative sensitivity, colour change

Posted Date: May 12th, 2026

DOI: https://doi.org/10.21203/rs.3.rs-9457832/v1

License: This work is licensed under a Creative Commons Attribution 4.0 International License.
Read Full License

Additional Declarations: No competing interests reported.

Version of Record: A version of this preprint was published at Journal of Fluorescence on June 30th, 2026. See the published version at https://doi.org/10.1007/s10895-026-04845-x.

Abstract

In this study, a highly sensitive fluorescence temperature sensing strategy accompanied by color change, based on thermal population and non-radiative transition, has been developed. To enhance the temperature sensitivity in high-temperature regions and to observe significant color changes with the naked eye, the fluorescence spectrum based on thermal population and non-radiative transition has been discussed and designed. The co-doped YVO_4:Tm^{3+}/Er^{3+} luminescent material was prepared by the high-temperature solid-phase method. Utilizing the strong absorption of ultraviolet (UV) by the V-O charge transfer band, the material was excited with 310 nm UV light. A significant color change from blue to blue-green and finally to green was achieved in the luminescent material within the temperature range of 450 K. The two fluorescence intensity ratios (*FIR*) were analyzed. In the high-temperature region, the *FIR* from the non-thermal coupling levels $^1G_4$ and $^2H_{11/2}$ satisfy the Boltzmann distribution. The relative sensitivity (S_r) reached its maximum at 583 K, with a maximum value of 1.74% K^{-1}. This strategy increased the sensitivity by 8.5 times at 583 K compared to the thermal coupling level temperature measurement strategy. A color transition recognizable by the naked eye was achieved within the 450 K range, demonstrating thermal anti-behavior, providing a reference for enhancing relative sensitivity in high-temperature regions.

1. Introduction

Accurate temperature measurement is crucial in fields like aerospace, medical technology, and scientific research. Rare-earth ion-doped materials have gained wide attention in non-contact thermometry[1–6]. These materials offer several excellent features. They provide high relative sensitivity and rapid response times. Moreover, they do not rely on the inherent emissivity of the object. They also do not disrupt the measured temperature field. Currently, thermometry systems use either thermally coupled levels (TCLs) or non-thermally coupled levels (NTCLs) [7, 8]. However, both systems rely on expensive spectral testing equipment. In contrast, color-recognition-based thermometry effectively reduces both device fabrication and practical application costs. This greatly broadens the application scenarios of fluorescence thermometry [9]. Therefore, developing new fluorescent materials based on color recognition is highly important. It has become a major research focus and a key challenge in the current field of non-contact fluorescence thermometry.

However, rare-earth ions naturally have many characteristic emission levels. This causes their emission spectra in the visible range to show multiple peaks. To some extent, this limits color recognizability during fluorescence thermometry. For example, Meng et al. developed Pr^{3+}-doped sensors that emit light in the red, green, yellow, and blue visible bands [10]. Singh K prepared Eu^{3+}-based materials with emission peaks covering the green, red, and yellow regions [11]. Ding et al. developed Er^{3+} upconversion materials that show dual emissions in both the red and green bands [12]. We believe that to specifically design color-recognition-based materials, we must systematically analyze the fundamental luminescence of rare-earth ions. Essentially, designing a temperature-dependent, color-recognizable sensor requires

focusing on three core aspects: First, we must carefully select two luminescent centers from rare-earth ions. Both must have excellent monochromatic emission in the visible range. Second, focusing on the overall relative sensitivity, we must independently analyze and synergistically control the emission properties of both centers. This helps build a stable, color-recognizable system. Third, to improve color recognition sensitivity, we must build a dual-center system with inverse thermally induced emission behaviors. This means as temperature rises, one color's intensity decreases while the other's increases. This process must consider the emission properties of both ions, with a special focus on their anti-quenching performance.

In this study, we developed a color-recognizable fluorescent thermometry material for the visible range. Based on a systematic analysis of emission mechanisms, we selected the characteristic emission levels of Tm^{3+} and Er^{3+} as the dual luminescent centers. We used yttrium vanadate (YVO_4) as the host. The target material was prepared using a high-temperature solid-state method. Through temperature-dependent emission spectra tests, we observed that Er^{3+} produces green fluorescence. This green emission shows anti-thermal quenching and its intensity increases as temperature rises. Meanwhile, the blue fluorescence of Tm^{3+} decays rapidly with increasing temperature. Thus, we successfully built a dual-center system with inverse thermally induced emission behaviors.

We quantitatively analyzed the fluorescence intensity ratio (FIR) of the dual centers. This provided an FIR-temperature calibration curve for temperature detection. We further analyzed key performance parameters, including absolute sensitivity Sa, relative sensitivity Sr, and temperature uncertainty ΔT. Based on this, we imported the temperature-dependent fluorescence spectral data into a chromaticity diagram for colorimetric analysis. We calculated the theoretical emission color at each temperature. We then compared and verified these calculations with the actual colors photographed in our experiments. We successfully achieved a continuous and reversible color change from blue to blue-green, and finally to green, in the temperature range of 323 K to 773 K. This study provides an important experimental and theoretical basis for the future targeted design of highly sensitive, color-recognizable fluorescent thermometry materials.

2. Experiments and Tests

The YVO_4:2% Tm^{3+} 0.5% Er^{3+} samples were synthesized using a high-temperature solid-state method. The precursor materials included Er_2O_3, Tm_2O_3, Y_2O_3, and NH_4VO_3 (99.99% purity, Aladdin). First, stoichiometric amounts of these powders were accurately weighed using an electronic balance. They were then thoroughly ground for 1 hour to ensure uniform mixing. Next, the mixed powder was calcined in a muffle furnace at 1000°C for 6 hours. To evaluate the fluorescence properties, the prepared samples were pressed into pellets. The excitation and emission spectra were measured using a fluorescence spectrometer (Zolix Instruments Co., Ltd.). This spectrometer was equipped with a 450 W xenon lamp as the excitation source.

3. Results and discussion

Analyzing the fluorescence behavior of dual-emitting centers requires understanding their excitation processes. Figure 1(a) illustrates the specific excitation and de-excitation pathways. Under 310 nm ultraviolet (UV) excitation, electrons transition from the ground state to the excited state. This occurs through the charge transfer band (CTB) of the V-O bonds. Figure 1(b) presents the excitation spectra of YVO_4:Er^{3+}/Tm^{3+}, monitored at 474 nm corresponding to the characteristic $^1G_4$ emission of Tm^{3+}, and at 550 nm corresponding to the $^4S_{3/2}$ emission of Er^{3+}.Following this, the absorbed energy is transferred to the excited states of the rare-earth ions (Tm^{3+} and Er^{3+}) via energy transfer. Finally, due to the crystal field effect, these excited rare-earth ions return to their ground states. This relaxation happens through either radiative or non-radiative transitions. This complete cycle defines the excitation and de-excitation processes of the material.

To verify the thermal and fluorescence behaviors of the co-doped ions, variable-temperature emission spectra were measured. As shown in Fig. 2, the samples were excited at 310 nm via the strong absorption of the V-O bond. This excitation produced a strong blue emission from the $^1G_4 \rightarrow {}^3H_6$ transition of Tm^{3+}. It also produced weak green emissions from the $^2H_{11/2} \rightarrow {}^4I_{15/2}$ and $^4S_{3/2} \rightarrow {}^4I_{15/2}$ transitions of Er^{3+}. As the temperature increases, the $^1G_4 \rightarrow {}^3H_6$ blue emission quenches rapidly. For Er^{3+}, the $^2H_{11/2} \rightarrow {}^4I_{15/2}$ green emission initially increases and then decreases due to thermal population effects. Meanwhile, the $^4S_{3/2} \rightarrow {}^4I_{15/2}$ emission steadily decreases. We attribute the weakening of the Tm^{3+} blue emission to two combined factors. These are the weakened absorption of the V–O bond and enhanced non-radiative transitions. The Er^{3+} green emission is also affected by these same processes. However, there is an energy gap of approximately 850 cm^{-1} between the $^2H_{11/2}$ and $^4S_{3/2}$ levels. Because of this gap, strong thermal population occurs. This thermal population partially offsets the fluorescence quenching effect. As a result, it enables a stronger thermal anti-quenching behavior. Both the strong blue and weak green emissions maintain good monochromaticity. However, a minor red emission is observed near 650 nm. This red emission also originates from the $^1G_4$ level of Tm^{3+}. Its intensity is low, and it quenches rapidly as the temperature rises. Therefore, it does not significantly affect the overall color transition in the visible range.

To further analyze the thermal behavior, we calculated the integrated intensities of the three main emissions. Figure 3 illustrates these changes with temperature. Blue dots ($^1G_4 \rightarrow {}^3H_6$ of Tm^{3+}): This blue emission quenches significantly as the temperature rises. Notably, at 623 K, its intensity drops below the sum of the green emissions. This suggests the overall emission theoretically begins to change from blue to green in this range. At 743 K and 773 K, the blue emission becomes weaker than each individual green emission. This indicates a complete theoretical transition to a green color. Dark green dots ($^2H_{11/2} \rightarrow {}^4I_{15/2}$ of Er^{3+}): This emission strengthens as the temperature increases from 323 K to 573 K. This happens due to the thermal population from the $^4S_{3/2}$ level. From 573 K to 773 K, the intensity decreases. However, it remains stronger than its initial value at 323 K. This overall trend results from the

combined effects of thermal population and non-radiative transitions. Light green dots ($^4S_{3/2} \rightarrow {}^4I_{15/2}$ of Er^{3+}): This emission shows a continuous decrease in fluorescence intensity as the temperature increases. As mentioned earlier, the $^2H_{11/2}$ and $^4S_{3/2}$ levels of Er^{3+} are a pair of thermally coupled levels (TCLs). Therefore, the intensity ratio of I_2 to I_3 is expected to follow the Boltzmann distribution.

To further understand the fluorescence intensity ratio (FIR) of the energy levels, we applied two different strategies across different temperature ranges. As shown in Fig. 4, we first analyzed the FIR (I_2/I_3) of the thermally coupled levels (TCLs) in a lower temperature range (323 K to 623 K). Then, we analyzed the FIR (I_2/I_1) of the non-thermally coupled levels (NTCLs) in a higher temperature range (593 K to 773 K). For TCLs, the particle population ratio between the two levels naturally follows the Boltzmann distribution. Similarly, for NTCLs, we hypothesize that their FIR also follows a Boltzmann-type distribution at high temperatures due to non-radiative transitions. To verify this, we fitted the temperature-dependent FIR data using the following equation [13, 14]:

$$R = B\exp\left(-\frac{\Delta E}{kT}\right)$$

1

,

In Eq. (1), *R* represents the fluorescence intensity ratio. *B* is a constant related to the degeneracy of the energy levels. ΔE is the effective energy difference. *k* is the Boltzmann constant (with a value of 0.695 $cm^{-1} K^{-1}$, and *T* is the absolute thermodynamic temperature.

As shown in Fig. 4, the FIR (I_2/I_3) of the TCLs strictly follows the Boltzmann distribution between 323 K and 623 K. The fitting result yields ΔE/k = 1225 K^{-1}. This value is highly consistent with the actual energy gap between the $^2H_{11/2}$ and $^4S_{3/2}$ levels in singly Er^{3+}-doped systems [15]. Between 593 K and 773 K, the FIR (I_2/I_1) of the NTCLs also shows an excellent Boltzmann fit. This fitting gives ΔE/k = 8828 K^{-1}. Notably, for NTCLs, this value does not represent a physical energy gap between the two emission levels. Rather, it indicates that the overall luminescence kinetics satisfy a Boltzmann distribution. In this temperature range, the $^1G_4$ level of Tm^{3+} experiences severe non-radiative transitions. Simultaneously, the upper level of Er^{3+} is populated by thermal excitation from its lower level. These combined thermal effects drive the system to follow this distribution.

To further evaluate the temperature sensing performance of thermally coupled and non-thermally coupled systems, the relative sensitivity was examined. The relative sensitivity *S*r is defined as [16, 17]:

$$S_r = \frac{1}{R}\frac{dR}{dT} \times 100\%.$$

2

Figure 5 presents the relative sensitivity curves derived from the two fluorescence intensity ratio (FIR) fits. For the thermally coupled system, the maximum relative sensitivity occurs at 323 K, reaching 0.83% K^{-1}. As is typical for thermally coupled-based thermometers, *S*r decreases monotonically with increasing temperature. While the sensitivity is relatively high near room temperature, it declines to below 0.2% K^{-1} at 623 K, consistent with theoretical predictions. This sensitivity can be partially enhanced by enlarging the energy gap between the thermally coupled levels.

For the non-thermally coupled system, the maximum relative sensitivity is attained at 583 K, with a value of 1.74% K^{-1}. This result indicates superior performance of NTC thermometry in the high-temperature regime. In the Tm^{3+}/Er^{3+} co-doped host, the $^1G_4$ level of Tm^{3+} undergoes strong thermal quenching at elevated temperatures due to enhanced non-radiative relaxation. The $^2H_{11/2}$ level of Er^{3+} is subject to the same quenching mechanisms. However, thermal population from the lower-lying $^4S_{3/2}$ level offsets this quenching, sustaining the green emission intensity. The contrast between severe blue quenching and moderate green attenuation drives the observed chromatic transition.

The realization of visually discernible color shifts over a limited temperature span is of considerable practical importance. Such behavior requires several conditions as below: distinct thermal quenching rates between the two emitting centers, sufficient spectral separation between their emission bands, and minimal interference from parasitic radiative transitions. In contrast to upconversion processes, where multiphoton excitation populates multiple emitting states in both Tm^{3+} and Er^{3+}, the down-conversion luminescence of Tm^{3+}/Er^{3+} in the YVO_4 matrix exhibits excellent monochromaticity. Using the CIE 1931 standard colorimetric system, the emission spectra were converted into chromaticity coordinates [18–20]. Figure 6 shows a pronounced color evolution—from blue to blue-green, and finally to green—is observed across the temperature range of 323– 773 K. The transition becomes particularly evident beyond 593 K, corroborating the relative sensitivity analysis.

4. Conclusions

In summary, a sensitive fluorescence thermometry strategy based on thermal population and non-radiative transitions was demonstrated in YVO_4:Tm^{3+}/Er^{3+}. The material exhibits a continuous color change from blue (323 K) to blue-green, then to green (773 K), driven by the strong thermal quenching of Tm^{3+} blue emission and the anti-thermal behavior of Er^{3+} green emission. FIR analysis shows that both thermally coupled ($^2H_{11/2}/^4S_{3/2}$) and non-thermally coupled ($^1G_4/^2H_{11/2}$) level pairs follow a Boltzmann-type temperature dependence. The relative sensitivity reaches 0.83% K^{-1} at 323 K for the thermally coupled system and 1.74% K^{-1} at 593 K for the non-thermally coupled system, an 8.5-fold enhancement over conventional thermally coupled thermometry. This dual-center design enables visually discernible color transitions over a 450 K span and provides a viable pathway for high-sensitivity optical thermometry in elevated-temperature regimes.

Declarations

Disclosures.

The authors declare no conflicts of interest.

Funding.

Supported by the Project of Basic Scientific Research Funds of Heilongjiang Education Department (Grant Nos. YWF10236250214)

Author Contribution

Zhensheng Lu and Changwen Wang wrote the main manuscript text and Hongxia Tang and Meilin Song prepared figures. All authors reviewed the manuscript.

Data availability.

Data underlying the results presented in this paper are not publicly available at this time but may be obtained from the authors upon reasonable request.

References

1. Zhang B, Guo X, Zhang Z, Fu Z, Zheng H (2022) Luminescence thermometry with rare earth doped nanoparticles: Status and challenges. J Lumin 250:119110. https://doi.org/10.1016/j.jlumin.2022.119110
2. Maciel GS, Rakov N (2013) Anomalous up-conversion dynamics in rare-earth doped yttrium oxide powders. J Mater Chem C 1:3563–3568. https://doi.org/10.1039/c3tc00696d
3. Zhang C, Yang H, Zhang Y, Shang Y, Zhang X, Zhao LD, Gong S (2025) Development and application of rare earth-doped fluorescent thermometry materials. Sci China Mater 68:1702–1716. https://doi.org/10.1007/s40843-025-3286-2
4. Ao R, Xing LL, Yang W (2021) A high-brightness phosphor based on Yb^{3+}/Er^{3+} codoped Y_2O_3 micro-crystals and controllable temperature sensing sensitivity via rare earth ions. Opt Commun 492:126967. https://doi.org/10.1016/j.optcom.2021.126967
5. Li J, Xu S, Liu Y, Cao S (2024) Luminescent/temperature-sensing properties of multifunctional rare-earth upconversion Kevlar nanofiber composite under 1550 nm. Nanomaterials 14:740. https://doi.org/10.3390/nano14090740

6. Li M, Zhou X, Zhang Y, Jiang F, Sha S, Xu S, Li S (2020) Preparation and upconversion luminescent properties of Yb^{3+}/Er^{3+} doped transparent glass-ceramics containing CaF_2 nanocrystals. Ceram Int 46:25399–25404. https://doi.org/10.1016/j.ceramint.2020.07.008
7. Yin Q, Quan Y, Luo F, Gong W, Liu J, Chai J, Zhang L, Liu J (2025) Effect of excitation energy on the optical temperature sensing behavior of Dy^{3+} doped YSZ and YAG phosphors. Appl Mater Today 46:102889. https://doi.org/10.1016/j.apmt.2025.102889
8. Pang T, Mao J, Jian R, Guo H (2022) Effect of excitation energy on non-thermally coupled temperature sensing of $NaGdF_4:Yb^{3+}/Er^{3+}$ upconversion nanocrystals. J Lumin 248:118980. https://doi.org/10.1016/j.jlumin.2022.118980
9. Zhang C, Yang H, Zhang Y, Shang Y, Zhang X, Zhao LD, Gong S (2025) Development and application of rare earth-doped fluorescent thermometry materials. Sci China Mater 68:1702–1716. https://doi.org/10.1007/s40843-025-3286-2
10. Yi L, Meng Q, Sun W (2025) Highly sensitive optical thermometry in Pr^{3+} doped $CaWO_4$ nanophosphors. Ceram Int 51:39587–39596. https://doi.org/10.1016/j.ceramint.2025.06.194
11. Singh K, Pradhan P, Priya S, Mund S, Vaidyanathan S (2023) Recent progress in trivalent europium (Eu^{3+})-based inorganic phosphors for solid-state lighting: an overview. Dalton Trans 52:13027–13057. https://doi.org/10.1039/d3dt00303e
12. Hu J, Wu Y, Duan B, Li Y, Wang F, Jin W, Ding C (2023) Enhanced upconversion luminescence and single-band red emission in β-Ba_2ScAlO_5: Yb^{3+}/Er^{3+} phosphor through doping Cu^{2+}. J Lumin 263:120053. https://doi.org/10.1016/j.jlumin.2023.120053
13. Wang C, Peng L, Qin F, Kou M, Wang Y, Xu L, Zhang Z (2024) A novel optical thermometry strategy: Based on the combined effects of red-shift charge transfer band and thermal coupling. J Lumin 275:120711. https://doi.org/10.1016/j.jlumin.2024.120711
14. Peng L, Qin F, Wang C, Li L, Zhang Z (2023) A high-precision thermometry strategy by replacing the infrared with visible light for detection. Opt Lett 48:4061–4064. https://doi.org/10.1364/OL.494971
15. Li Y, Su F, Cai Q, Guo H, Chai X, Zou H (2025) Yb and Re (Re = Er, Ho) codoped Sr_2ScSbO_6 double perovskites: dual-color upconversion luminescence for optical thermometry. J Mater Sci Mater Electron 37:14. https://doi.org/10.1007/s10854-025-16416-0
16. Zhu Y, Li C, Deng D, Yu H, Li H, Wang L, Shen C, Jing X, Xu S (2021) High-sensitivity based on Eu^{2+}/Cr^{3+} co-doped $BaAl1_2O_{19}$ phosphors for dual-mode optical thermometry. J Lumin 237:118142. https://doi.org/10.1016/j.jlumin.2021.118142
17. Chen B, Wang H, Wang B, Jing Z, Gao P, Tu G, Zong X, Tu B, Wang W, Fu Z (2024) A novel four-mode luminescent thermometry by employing cross-relaxation of upconversion fluorescence in Er^{3+}-doped MgAlON transparent ceramics grain boundary. J Eur Ceram Soc 44:3180–3190. https://doi.org/10.1016/j.jeurceramsoc.2023.12.084

18. Li X, Meng Q, Sun W (2025) The optical temperature sensing based on FIR of YVO_4: Bi^{3+}, Sm^{3+} nanophosphors. J Lumin 287:121491. https://doi.org/10.1016/j.jlumin.2025.121491
19. Li X, Meng Q, Lan Q (2025) Highly sensitive optical temperature sensing based on FIR of $CaWO_4$: Sm^{3+} nanophosphor. Adv Mater Technol 10:2500042. https://doi.org/10.1002/admt.202500042
20. Yin S, Meng Q (2025) Optical thermometry based on different luminescence thermal responses of matrix and doped ions in $CaMoO_4$: Sm^{3+} phosphors. J Photochem Photobiol A 459:116044. https://doi.org/10.1016/j.jphotochem.2024.116044

Figures

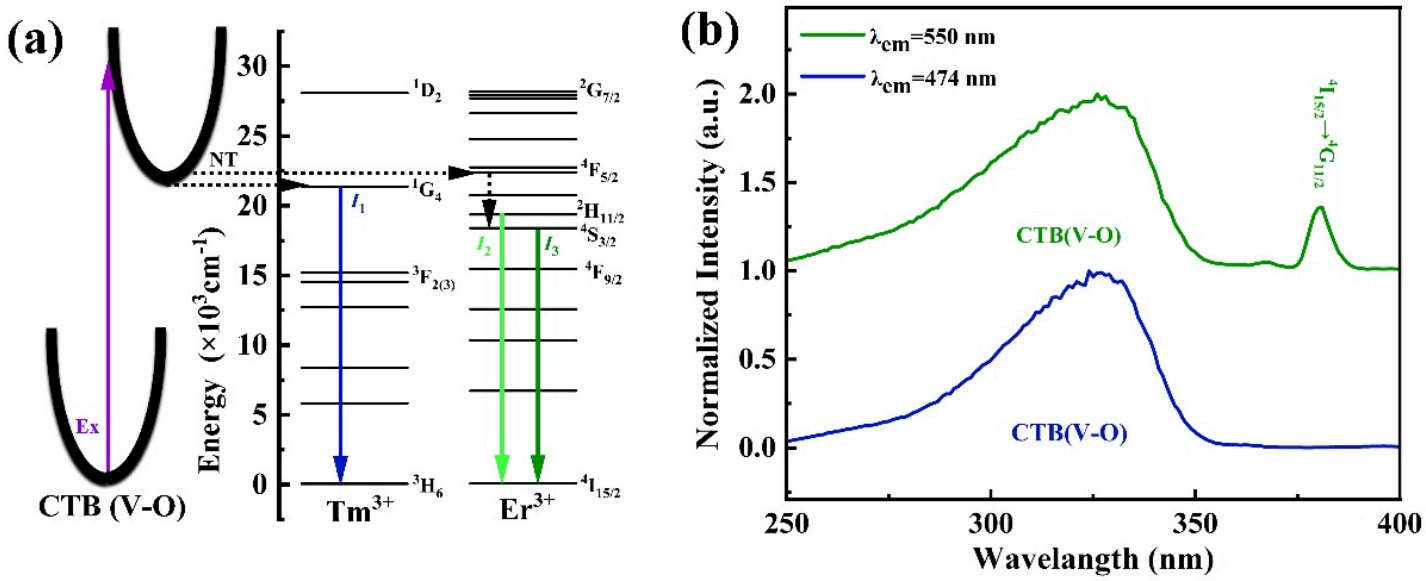


Figure 1

(a) Schematic diagram of the V-O charge transfer band, energy level diagrams of Tm^{3+} and Er^{3+}. (b) Excitation spectrum of YVO_4:Er^{3+}/Tm^{3+}

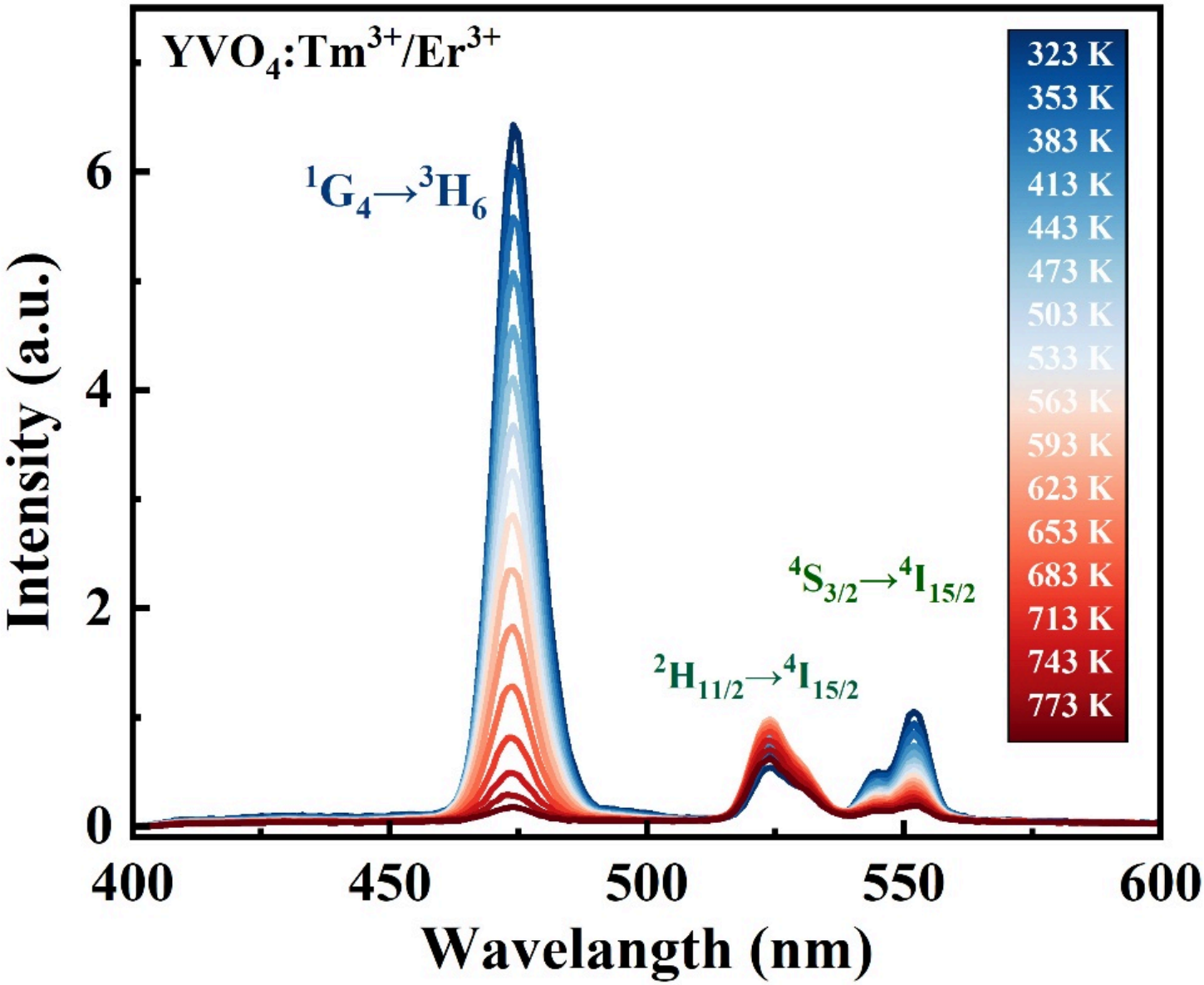


Figure 2

Temperature-dependent emission spectra of $YVO_4:Tm^{3+}/Er^{3+}$ co-doped material excited by 310 nm ultraviolet light, where the color transition from blue to red represents the temperature range from 323 K to 773 K.

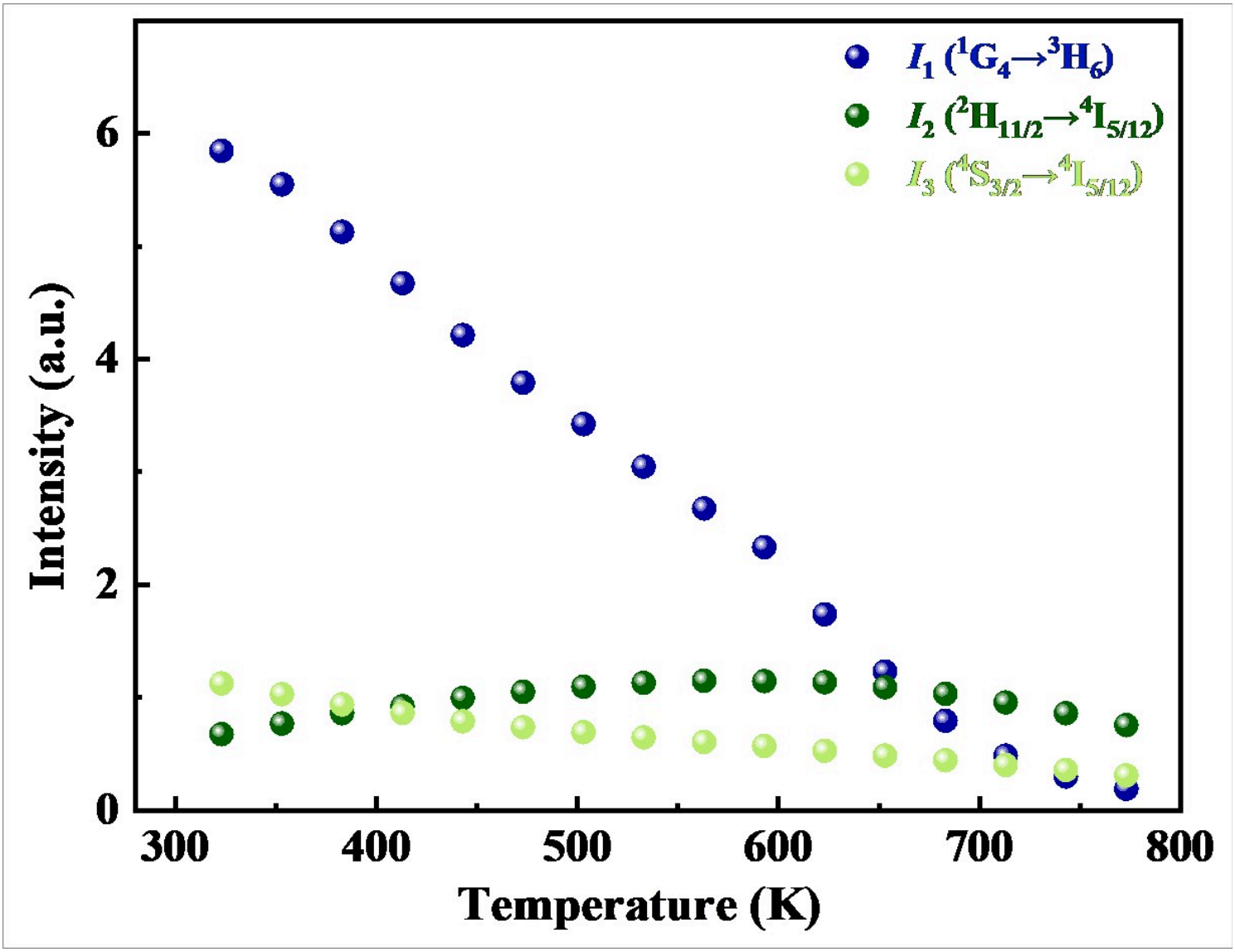


Figure 3

Temperature-dependent integrated emission intensities of I_1 ($^1G_4$-$^3H_6$), I_2 ($^2H_{11/2}$-$^4I_{15/2}$), and I_3 ($^4S_{3/2}$-$^4I_{15/2}$).

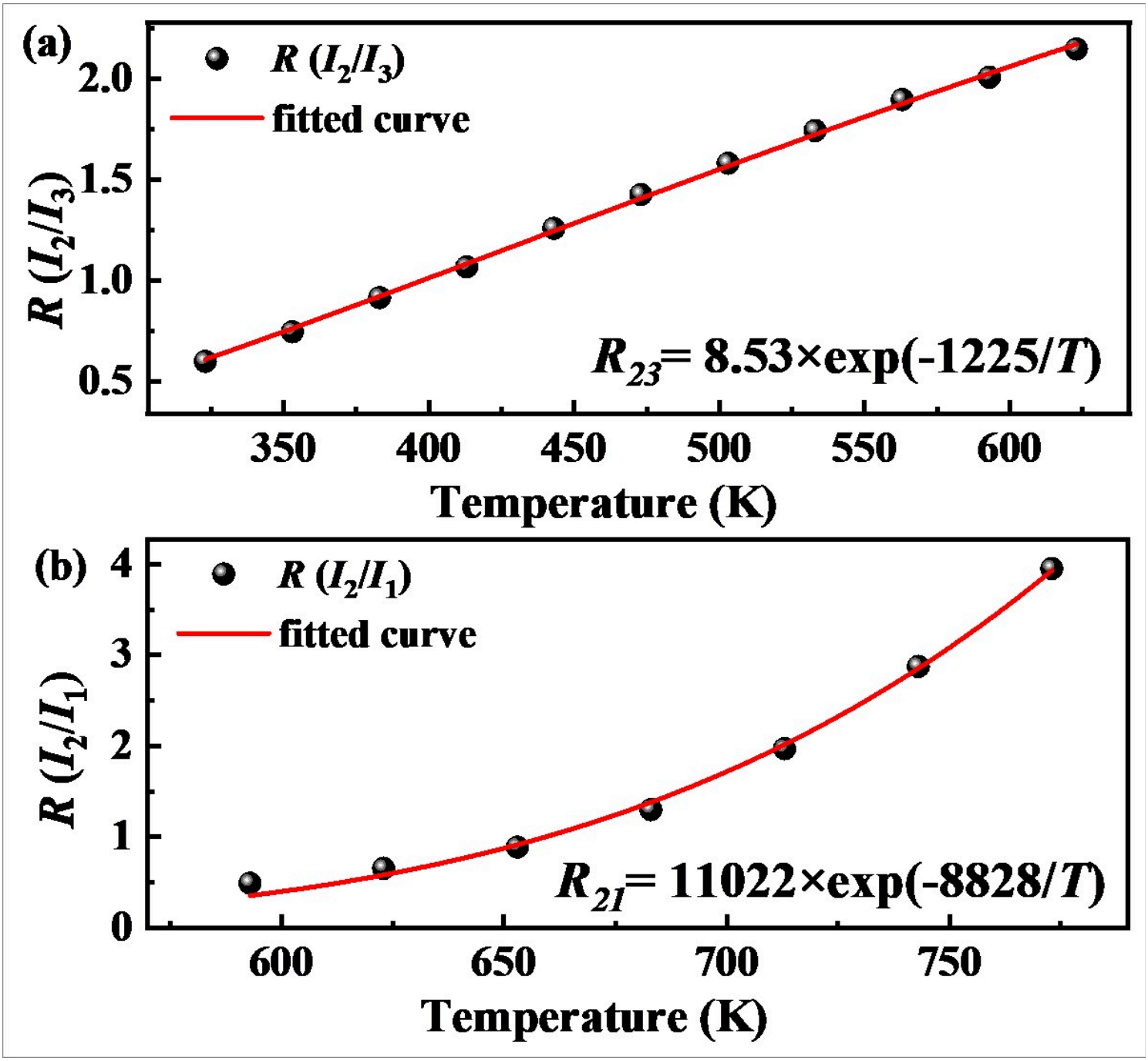


Figure 4

Fluorescence intensities ratio of (a) thermally coupled energy levels (I_2/I_3) in the lower temperature range (323 K – 623 K), and (b) non-thermally coupled energy levels (I_2/I_1) of in the higher temperature range (593K to 773K). Fitted curve based on fluorescence intensity ratio.

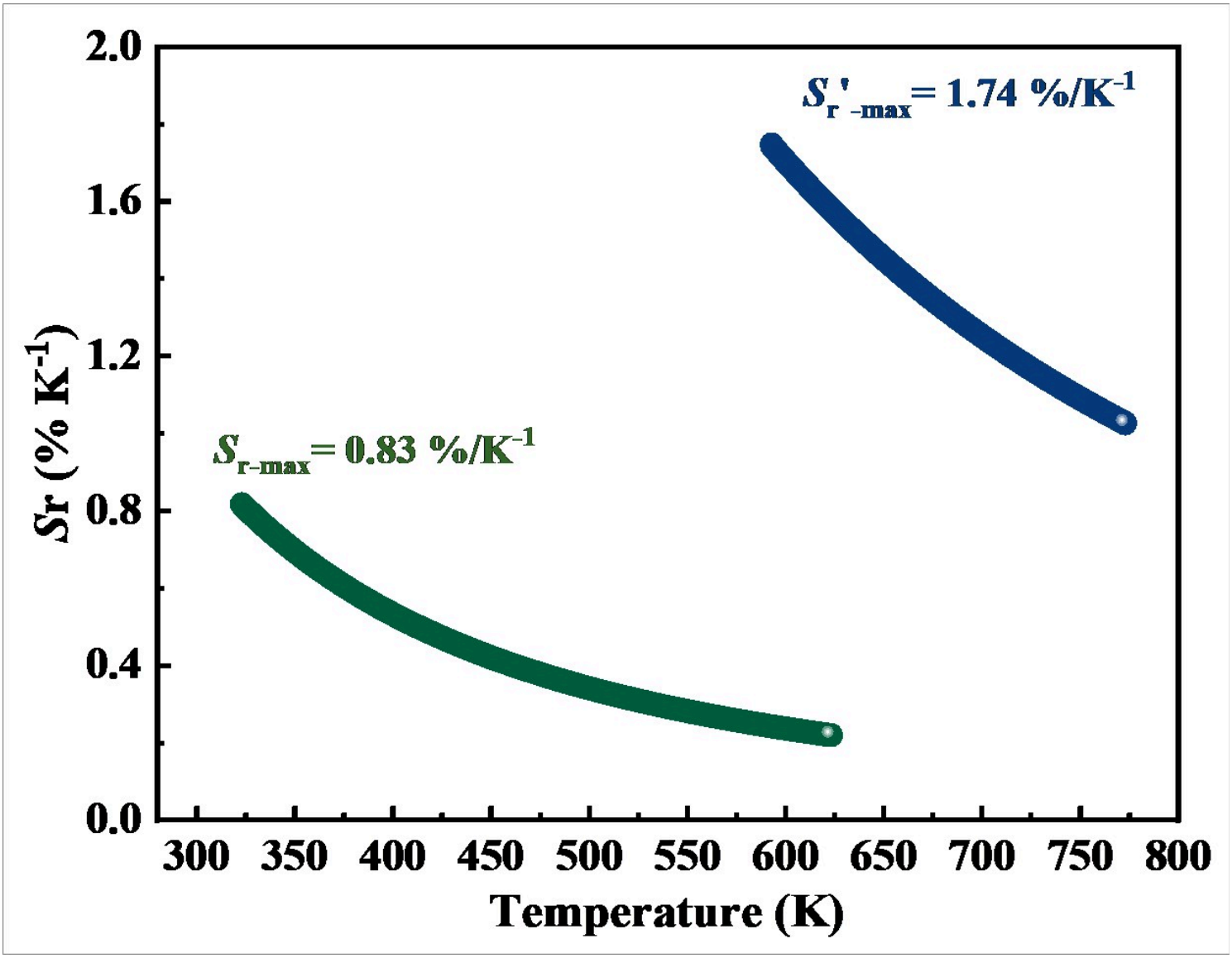


Figure 5

Relative sensitivity of $R(I_2/I_3)$ and $R(I_2/I_1)$

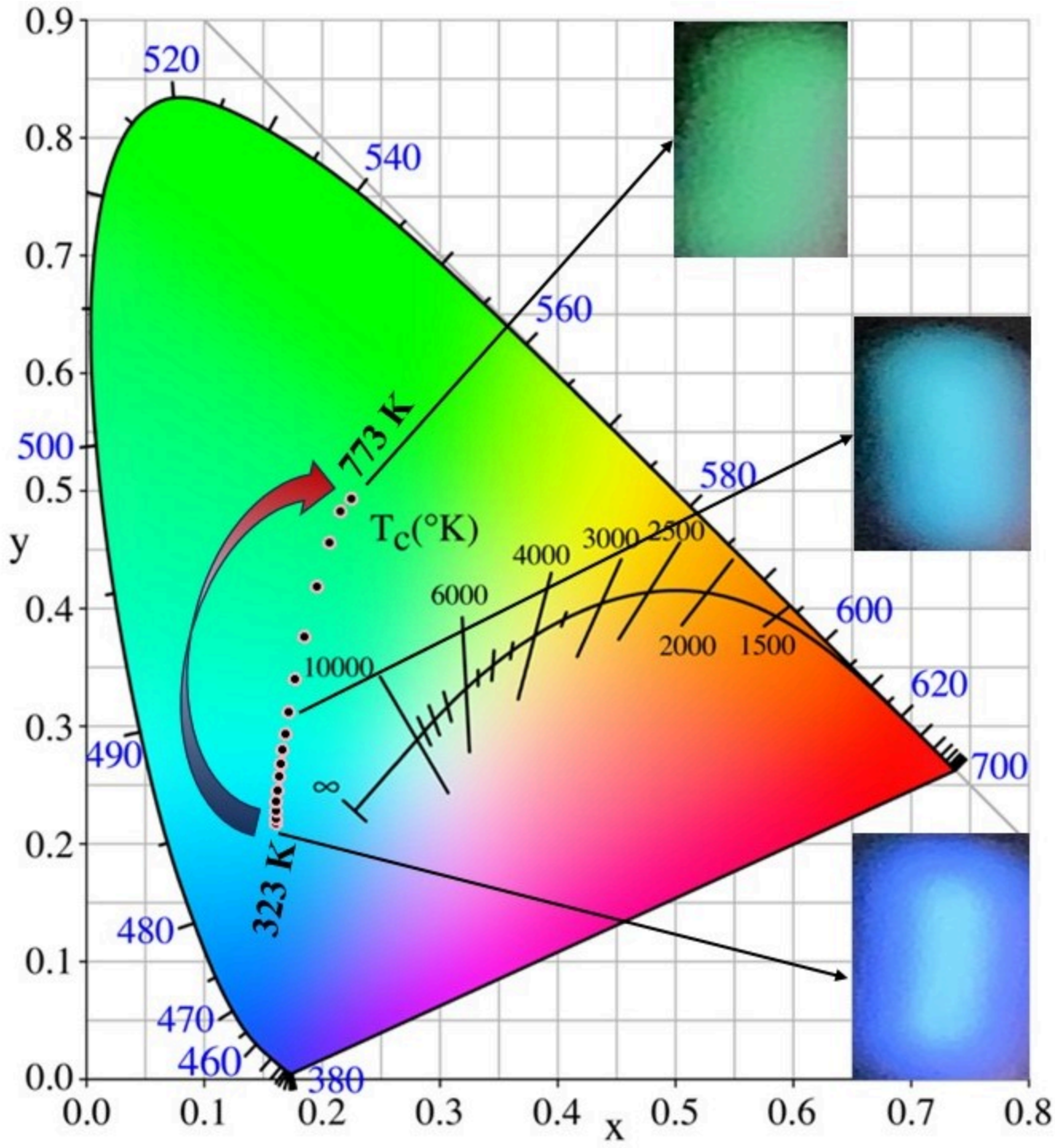


Figure 6

Color coordinates and color change process of YVO_4:Tm^{3+}/Er^{3+} co-doped luminescent materials at different temperatures. The insets are the luminescent colors of the samples photographed by a camera at temperatures of 323 K, 593 K, and 773 K.